

# RSC Advances



This is an *Accepted Manuscript*, which has been through the Royal Society of Chemistry peer review process and has been accepted for publication.

*Accepted Manuscripts* are published online shortly after acceptance, before technical editing, formatting and proof reading. Using this free service, authors can make their results available to the community, in citable form, before we publish the edited article. This *Accepted Manuscript* will be replaced by the edited, formatted and paginated article as soon as this is available.

You can find more information about *Accepted Manuscripts* in the [Information for Authors](#).

Please note that technical editing may introduce minor changes to the text and/or graphics, which may alter content. The journal's standard [Terms & Conditions](#) and the [Ethical guidelines](#) still apply. In no event shall the Royal Society of Chemistry be held responsible for any errors or omissions in this *Accepted Manuscript* or any consequences arising from the use of any information it contains.

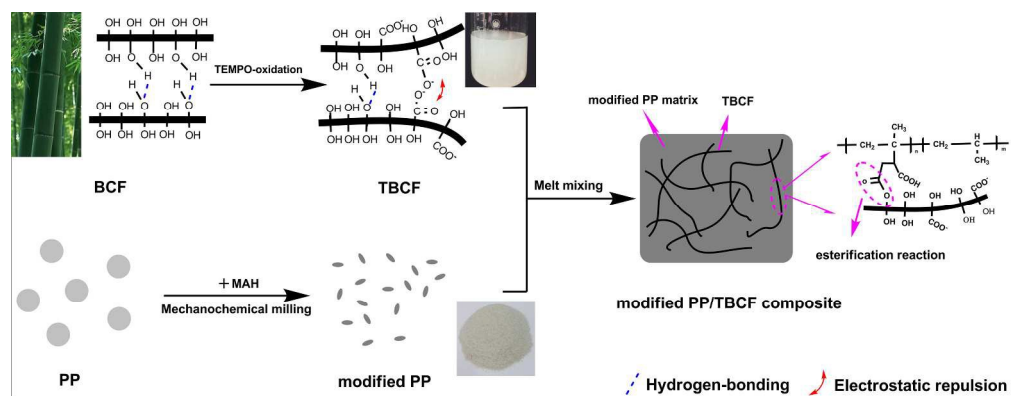


Fig. 1 Schematic illustration for the preparation of modified PP/TBCF composite through dual modification. 485x187mm (150 x 150 DPI)

1 **Towards mechanically robust cellulose fiber-reinforced**  
2 **polypropylene composites with strong interfacial interaction through**  
3 **dual modification**

4 **Shuman Wang, Yifeng Lin, Xinxing Zhang\* and Canhui Lu\***

5 *State Key Laboratory of Polymer Materials Engineering, Polymer Research Institute of Sichuan*  
6 *University, Chengdu 610065, China*

7 **Abstract:**

8 Strong interfacial interaction between bamboo cellulose fiber (BCF) and polymeric matrix is very  
9 important to improve the mechanical properties of cellulose fiber-reinforced polymeric composites.  
10 In this study, we developed an effective approach to enhance the interfacial adhesion through  
11 modifying both polypropylene (PP) and cellulose fiber. Maleic anhydride was mechanochemically  
12 grafted onto PP to achieve the interaction with the reactive hydroxyl groups on the surface of  
13 2,2,6,6-tetramethylpiperidine-1-oxy radical (TEMPO)-oxidized bamboo cellulose fiber (TBCF).  
14 Fourier transform infrared spectra and X-ray diffraction analysis indicated the existence of strong  
15 interfacial interaction between TBCF and the modified PP matrix. It was further quantified by  
16 thermogravimetric analysis that about 5 wt% of PP formed a strong combining force with TBCF  
17 after melt compounding. The combination of mechanochemical modification of PP and  
18 TEMPO-mediated oxidation of BCF showed a synergistic effect on the tensile strength of the  
19 prepared composites. The tensile strength of modified PP/TBCF (50/50 wt%) composites prepared  
20 through dual modification was remarkably improved compared to those of neat PP/TBCF

---

\*Corresponding author: Xinxing Zhang and Canhui Lu

E-mail address: [xxzwwh@126.com](mailto:xxzwwh@126.com) and [canhuilu@scu.edu.cn](mailto:canhuilu@scu.edu.cn)

Tel: +86-28-85460607 Fax: +86-28-85402465

21 composites and modified PP/BCF composites, enhanced by about 112.4% and 53.8%,  
22 respectively.

23

24 Keywords: polypropylene; cellulose fiber; composites; surface modification; interfacial interaction

25

## 26 **1. Introduction**

27 Cellulose is one of the most abundant, renewable and biodegradable natural polymers  
28 existing in wood, bamboo, cotton, hemp, straws, sugarcane bagasse and other plants.<sup>1-3</sup> Recently,  
29 the emphasis on sustainable and environmentally friendly materials has steered the trend of  
30 incorporating natural cellulose fiber into polymeric composites.<sup>4-6</sup> There are some problems faced  
31 by researchers in this field, most of them are related to the highly polar surface of cellulose, which  
32 causes its low interfacial compatibility with non-polar polymeric matrices and the ensuing fiber  
33 aggregation.<sup>7</sup> Numerous strategies have been developed to overcome these problems.<sup>8</sup> Typically,  
34 the use of coupling agents and the esterification of cellulose with fatty acids are two major  
35 approaches to improve interfacial interaction between cellulose and polymeric matrices.

36 In general, the Young's modulus of polymers can be increased by the reinforcement of  
37 cellulose, while the tensile strength does not improve or sometimes decreases due to the poor  
38 interfacial interaction even after modification.<sup>9</sup> For example, Qiu et al.<sup>10</sup> studied the effect of  
39 maleated polypropylene (MAPP) on the performance of polypropylene (PP)/cellulose composites.  
40 The addition of MAPP improved the interfacial adhesive between cellulose and PP matrix to some  
41 extent. But the tensile strength of the PP/cellulose (60/30 wt%) composites containing 10 wt%

42 MAPP only slightly increased comparing with that of neat PP. Similarly, Mulinari et al.<sup>11</sup> reported  
43 that the incorporation of zirconium oxychloride-treated sugarcane bagasse cellulose had a negative  
44 effect on the tensile strength of high density polyethylene. This drawback was also proved by  
45 Fávvaro et al.'s work<sup>12</sup>. The surface acetylation of rice husk fibers as a strategy produced  
46 polyethylene (PE)/rice husk composites with improved modulus, while the modified rice  
47 husk-filled composites showed lower tensile strength than that of neat PE.

48 To our best knowledge, modification of both cellulose and polymeric matrices has not been  
49 investigated in depth so far, as there are only limited reports about it. For example, Iwamaoto et  
50 al.<sup>13</sup> realized homogeneous filler dispersion in the PP/cellulose composites with the combination  
51 of added MAPP and cellulose surface-coating, leading to higher Young's modulus and tensile  
52 strength than those of neat PP. However, harmful reagents (e.g. toluene) were repeatedly used in  
53 these pretreatments, which might hinder their large-scale applications.

54 In this work, we investigated that the synergistic effect of mechanochemical modification of  
55 PP and 2,2,6,6-tetramethylpiperidine-1-oxy radical (TEMPO)-mediated oxidation of cellulose on  
56 the interfacial interaction and mechanical properties of PP/cellulose composites. Derived from the  
57 traditional Chinese stone-mill, the innovative pan-mill equipment is efficient in triggering  
58 mechanochemical reactions due to its three-dimensional scissor structure.<sup>14-16</sup> The self-designed  
59 pan-mill type mechanochemical reactor was employed to pulverize and modify the surface of PP  
60 powders simultaneously via mechanochemical reaction with maleic anhydride (MAH) in solid  
61 state. TEMPO-oxidation promoted cellulose fibrillation by selectively converting the surface  
62 hydroxyl moieties of cellulose into carboxylic groups and released reactive hydroxyl groups on  
63 the surface of cellulose, thereby enhancing the interfacial adhesion between cellulose and PP

64 matrix. The synergistic effect of mechanochemically modified PP and TEMPO-oxidized bamboo  
65 cellulose fiber (TBCF) on the interfacial interaction between cellulose and PP matrix was  
66 examined. In contrast to the previous works<sup>11, 12, 17</sup> where cellulose rarely showed reinforcing  
67 effect on the tensile strength of polymeric composites, the prepared modified PP/TBCF  
68 composites with high filler loading ( $\geq 50$  wt%) in this study showed a remarkably improved  
69 tensile strength comparing to that of neat PP due to the enhanced interfacial interaction. This new  
70 process is highly attractive and ready for large-scale applications.

## 71 **2. Experimental**

### 72 **2.1 Materials**

73 The raw material of bamboo cellulose fiber (BCF) with solid content of 28-32 wt% used in  
74 this study was supplied by Yongfeng Paper Co., China. PP homopolymer T30S was purchased  
75 from Lanzhou Petrochemical Industrial Company, China. It had a melting temperature of 165 °C  
76 and a melt flow index (MFI) of 3.2 g/10 min (2.16 kg at 230 °C). The TEMPO, sodium bromide  
77 (NaBr), sodium hypochlorite (NaClO), MAH and dimethylbenzene were purchased from Chengdu  
78 Kelong Inc., China. All reagents were of analytical grade and distilled water was used for the  
79 preparation of all solutions.

### 80 **2.2 Mechanochemical modification of PP via pan-milling**

81 Mechanochemical modification of PP was performed using the pan-mill type  
82 mechanochemical reactor. The details of the pan-mill equipment and operation procedure were  
83 depicted in our previous publications.<sup>18, 19</sup> Generally, a mixture of PP/MAH with weight ratio of  
84 100/7.5 was fed into hopper set at the middle of the moving pan. Milled powder was discharged  
85 from the brim of the pans. The discharged powder was then collected for the next milling cycle.

86 The whole milling process was conducted at a rotating speed of 60 rpm under ambient  
87 temperature. The obtained powder was Soxhlet extracted with water for 72 h to ensure thorough  
88 removal of residual MAH for subsequent analysis. Then, the modified PP powder product was  
89 dried in an electric oven at 60 °C. Neat PP pellets were milled at the same way as a comparison.

### 90 **2.3 TEMPO-mediated oxidation of cellulose**

91 BCF was pretreated by TEMPO-mediated oxidation method. NaBr (1 mmol per gram of  
92 cellulose) and TEMPO (0.1 mmol per gram of cellulose) were added to the suspension of bamboo  
93 pulp with the concentration of pulp in water was 2 wt%. Then NaClO (5 mmol per gram of  
94 cellulose) was added slowly to the suspension. The pH of the mixture was maintained to 10 at  
95 room temperature by adding 0.5 M sodium hydroxide (NaOH) and 0.5 M hydrochloric acid (HCl)  
96 while stirring the suspension. After all NaClO was consumed and pH kept still, the cellulose was  
97 washed thoroughly with deionized water until the filtrate solution was neutral. The products were  
98 filtered and dried at 60 °C in an electric oven to obtain the TBCF with about 30 wt% solid content.

99 The carboxylate content of the TBCF was determined by conductometric titration method.<sup>20</sup>  
100 The dry sample (1 g) was soaked in 100 mL 0.001M sodium chloride solution in the presence of  
101 magnetic stirring, then added with 0.1M HCl to set the pH value in the range of 2.5-3.0. A 0.1M  
102 NaOH solution was added at the rate of 0.1 mL/min up to pH 11 by pH meter. The total content of  
103 the TBCF was calculated from:

$$104 \quad \text{The carboxylate content (mmol/g)} = [(V_1 - V_0) \times C_{\text{NaOH}} \times 1000] / m_0$$

105 where  $V_1$  and  $V_0$  are the consumed volume of NaOH solution at the equivalent point, respectively,  
106 and  $m_0$  is the weight of dried product.

### 107 **2.4 Preparation of PP/cellulose composites**

108 In order to investigate the interfacial interaction between cellulose and polymeric matrix,  
109 modified PP/TBCF (10-60 wt% related to total weight) composites were prepared. Meanwhile,  
110 neat PP/TBCF composites and modified PP/BCF composites were obtained as comparison. The  
111 cellulose fiber with about 30 wt% solid content and PP were premixed with a high speed agitator  
112 for uniform dispersion. The mixture was then kneaded by a twin-roller mixer Brabender  
113 Plasticorder (PLE-330, Brabender Co., Germany). Compounding was carried out for 20 min at a  
114 roller speed of 50 rpm at 180 °C, and water was removed at this stage. The melt compounded  
115 products were crushed into small pieces, then compressed at 180 °C and 10 MPa pressure for 8  
116 min. A schematic illustration of the composite preparation method is shown in Fig. 1.

## 117 **2.5 Characterization**

### 118 **2.5.1 Optical microscopy**

119 The morphologies of the modified PP powders and the TBCF were observed using an optical  
120 microscope (Leica DMLM) and captured by a digital imaging system. The PP powders and TBCF  
121 were suspended in ethanol and water, respectively, both with a concentration of 0.5 wt%. One  
122 drop of the diluted sample was dropped on a glass slide and stamped with a coverslip for the  
123 observation.

### 124 **2.5.2 X-ray photoelectron spectroscopy (XPS) analysis**

125 To investigate the structure changes of PP during mechanochemically milling with MAH, the  
126 pan-milled PP powder was Soxhlet extracted with water for 72 h and then dried at 80 °C. The neat  
127 PP and modified PP powders were characterized by XPS (ESCALab220I-XL electron  
128 spectrometer from VG Scientific using 300 W AlK $\alpha$  radiation) for element and chemical analysis.

### 129 **2.5.3 Measurement of grafting degree of the modified PP**

130 The neat PP and modified PP powders were purified using a precipitation method. About 3 g  
131 of powders were dissolved into 100 mL of refluxing xylene and precipitated into 500 mL of  
132 acetone. Then filtered, washed by acetone for three times and dried at 80 °C for 12 h in an electric  
133 oven. The grafting degree of the purified product was determined by chemical titration.<sup>21</sup> The  
134 average data were obtained from three replicates.

#### 135 **2.5.4 Water-contact angle measurement**

136 The hydrophilicities of the neat PP and modified PP membrane surface were characterized by  
137 water-contact angle measurement. A contact angle goniometer (OCA20, Dataphysics, Germany)  
138 equipped with a single-LED light source was used for imaging the liquid drop auto-dispersed on  
139 the sample surface. The drop image is then grabbed per 10 s to obtain dynamic contact angle data.

#### 140 **2.5.5 Fourier transform infrared spectroscopy (FTIR) analysis**

141 PP/cellulose composites were extracted with boiling dimethylbenzene for 120 h to remove  
142 the matrix resin. The obtained cellulose powder samples were analyzed by FTIR (Nicolet 560  
143 spectrometer, USA). The spectra were recorded from 4000 to 400  $\text{cm}^{-1}$  at a resolution of 2  $\text{cm}^{-1}$   
144 over 20 scans. The samples were completely dried in an oven before tested.

#### 145 **2.5.6 Scanning electron microscopy (SEM) analysis**

146 SEM (JSM-5900LV, JEOL) was employed to observe the morphology of cellulose in the  
147 composites. Standard specimens were cryogenically fractured in liquid nitrogen. Before observing,  
148 the fracture surface was sputter-coated with gold.

#### 149 **2.5.7 X-ray diffraction (XRD) analysis**

150 XRD patterns were collected on a Philips Analytical X'Pert X-diffractometer (Philips Co.,  
151 Netherlands), using Cu-K $\alpha$  radiation ( $k = 0.1540 \text{ nm}$ ) at an accelerating voltage of 40 kV and the

152 current of 40 mA. The data were collected from  $2\theta = 5-60$  with a step interval of  $0.03^\circ$ . The degree  
153 of crystallinity can be relatively expressed by the percentage crystallinity index (CrI). The  
154 equation used to calculate the CrI<sup>22</sup> was in the following form:

$$155 \quad \text{CrI} = [(I_{002} - I_{\text{am}}) / I_{002}] \times 100$$

156  $I_{002}$  and  $I_{\text{am}}$  are the count reading at peak intensity at  $2\theta$  close to  $22^\circ$  and  $18^\circ$ , representing  
157 crystalline part and amorphous part in cellulose, respectively.

### 158 **2.5.8 Thermal analysis**

159 Thermogravimetric analysis (TG) and derivative thermogravimetric analysis (DTG) were  
160 carried out with a TA-2000 analyzer (TA Instrument, USA) under nitrogen purge (flow rate about  
161 100 mL/min). The scanning rate of  $10^\circ\text{C}/\text{min}$  and temperature range of  $30-600^\circ\text{C}$  was used.  
162 About 5 mg of samples were placed in an open alumina crucible for characterization. All the  
163 samples were oven dried at  $60^\circ\text{C}$  for 24 h before testing.

### 164 **2.5.9 Tensile tests**

165 The stress–strain properties were measured according to the ASTM D 412-80 specification  
166 using dumb-bell test pieces on an Instron 5567 universal testing machine (Instron Co., Canton,  
167 USA) at a crosshead speed of  $50\text{ mm}/\text{min}$ . At least five measurements for each sample were made  
168 in order to eliminate experimental error.

## 169 **3. Results and discussion**

### 170 **3.1 Mechanochemical modification of PP**

171 Surface-modified PP powders were prepared through solid-state pan-milling PP pellets with  
172 MAH under ambient temperature. Optical micrograph (Fig. 2a) reveals that the PP pellets are  
173 effectively pulverized into small particles with a particle size of  $10\ \mu\text{m}$  or less after 10 cycles of

174 pan-milling. Furthermore, it acquired a rougher surface and a larger specific area after  
175 mechanochemical treatment, which would benefit its interfacial adhesion with fibers.<sup>23</sup>

176 The structure changes of PP before and after mechanochemical modification were  
177 characterized by XPS (as shown in Fig. 3). It can be seen that the oxygen content of modified PP  
178 surface is three times more than that of neat PP. The main peak appears at the binding energy of C  
179 1s in -CH<sub>2</sub>- is about 284.9 eV. In Fig. 3d, a weak peak can be observed at the binding energy of  
180 288.4 eV, which is ascribed to the -C=O bond.<sup>24</sup> Meanwhile, the grafting degree of the  
181 mechanochemically modified PP was measured by chemical titration method. The experiments  
182 were performed in triplicate and the average value was measured to be 1.4%, indicating the high  
183 efficiency of mechanochemical modification. These results indicate that the macromolecular  
184 radicals of PP initiated graft polymerization reaction with low molecular MAH monomers due to  
185 the strong squeezing force in both radial and tangential directions exerted by the pan-mill  
186 equipment.<sup>25, 26</sup>

187 The mechanochemical grafting of MAH onto PP may affect its polarity and hydrophilicity.  
188 Therefore, temperature-dependent contact angle measurements were carried out to investigate the  
189 variation of the surface hydrophilicity of PP. Fig. 4 shows the corresponding traces obtained for  
190 the dynamic contact angle measurements carried out with water placed on the surface of both  
191 samples. As expected, water wettability of PP increased after mechanochemical grafting of MAH  
192 due to the introduction of polar oxygen-contained groups. The mechanochemically modified PP  
193 presented a significantly higher level of water affinity than that of the neat PP. The average water  
194 contact angle at equilibrium of PP decreased from its original 113° to 90° after mechanochemical  
195 modification, indicating that the stress-induced mechanochemical modification of PP resulted in a

196 more hydrophilic surface and hence improved its compatibilization with the polar cellulose.

### 197 **3.2 Morphological development of PP/cellulose composites**

198 In order to promote the interfacial interaction between cellulose and PP matrix, the BCF was  
199 pretreated with a TEMPO-mediated oxidation process. This process converted hydroxyl groups  
200 into carboxylic groups, generating electrostatic repulsion that favor the breakdown of the cohesion  
201 among the nanofibrils held by hydrogen bonding and released more reactive hydroxyl groups  
202 throughout the surface of cellulose.<sup>27,28</sup> The optical microphotograph of the TBCF is shown in Fig.  
203 2b. The TBCF is swollen in water and some individual nanofibrils appear on the surface of fiber,  
204 indicating nanofibrils and aggregates were gradually loosened from the fiber surface after  
205 TEMPO-oxidation pretreatment. Similar results were reported by Saito et al.<sup>29</sup> and Chen et al.<sup>30</sup>.

206 After TEMPO-oxidation pretreatment, the TBCF were melt-compounded with PP matrix in a  
207 melt mixer at 180 °C. The SEM images of the fractured surfaces of the composites with 30 wt%  
208 cellulose are shown in Fig. 2c, d and e, respectively. It can be seen from Fig. 2c that there are  
209 many pulled-out fibers in the fractured surface of neat PP/TBCF composites. Furthermore, the  
210 dispersion of TBCF are not uniform and aggregates of fibers can be found obviously in the neat  
211 PP matrix, indicating the poor interfacial compatibility of TBCF and neat PP matrix. In Fig. 2d,  
212 the interfacial boundary and the voids left on the fracture surface of modified PP/BCF composites  
213 are distinct. The large voids around the fibers demonstrate the weak adhesion at modified PP and  
214 BCF interfaces. It is apparent that the synergistic effect of the mechanochemically modified PP  
215 and TBCF improved the interfacial adhesion as the TBCF are almost completely embedded within  
216 the matrix (as shown in Fig. 2e). In addition, the TBCF are rather well distributed in the modified  
217 PP matrix. The same types of fracture surfaces were seen in the plasticized xylan/nanofibrillated

218 cellulose composites, in which no nanofibrils were pulled out from the matrix during fraction due  
219 to the strong interfacial interaction between cellulose and matrix.<sup>31</sup>

### 220 **3.3 Structure changes of cellulose before and after melt compounding**

221 One of the primary purposes of this study is to evaluate the effect of mechanochemical  
222 modification on the interfacial interaction between PP and cellulose. In order to verify their strong  
223 interfacial adhesion, the structure changes of cellulose before and after melt compounding with PP  
224 were investigated in detail. The PP/cellulose composites were Soxhlet extracted for 120 h using  
225 dimethylbenzene as a solvent to ensure thorough removal of the PP resins in composites and then  
226 the obtained residue was collected for characterization.

227 Fig. 5 shows the FTIR spectra of TBCF (a), TBCF extracted from neat PP/TBCF composites  
228 (b) and modified PP/TBCF composites (c). All spectra are normalized to the reference peak at  
229  $1033\text{ cm}^{-1}$  which is assigned to C-O stretching vibration of the cellulose backbone.<sup>31</sup> The FTIR  
230 spectrum of TBCF extracted from neat PP/TBCF composites is almost the same as that of the  
231 original TBCF. However, it is very interesting to note that although the mechanochemically  
232 modified PP was removed in the same way as the neat PP, the FTIR spectrum of the TBCF  
233 extracted from modified PP/TBCF composites presents as a superposition of the FTIR curves of  
234 cellulose and PP. The strong and sharp adsorption peaks at  $2917$  and  $1384\text{ cm}^{-1}$  are attributed to  
235 the  $\text{CH}_2$  stretching vibration and methyl symmetric bending vibration of PP, respectively.<sup>33</sup> The  
236 results indicate that there are strong interfacial interactions between mechanochemically modified  
237 PP and TBCF after melt compounding.

238 The enhanced interfacial adhesion may be a result of the esterification reaction between MA  
239 moieties and hydroxyl groups on the surface of cellulose.<sup>34-36</sup> The TEMPO-mediated oxidation

240 process contributed to the breakdown of intra- and intermolecular hydrogen bonds, releasing  
241 reactive hydroxyl groups on the surface of cellulose. Conductometric titration measurement  
242 indicates that the carboxylate content of TBCF is within the range of 0.8-1.0 mmol/g, confirming  
243 the generation of reactive hydroxyl groups. MA moieties of modified PP create chemical bonds  
244 with the exposed reactive hydroxyl groups on the surface of cellulose and establish strong  
245 interfacial interaction.

246 Fig. 6 presents the XRD patterns of TBCF (a), TBCF extracted from neat PP/TBCF  
247 composites (b), TBCF extracted from modified PP/TBCF composites (c) and BCF extracted from  
248 modified PP/BCF composites (d). All of the products maintained the original cellulose I crystal  
249 structure.<sup>37</sup> The crystallinity index of four kinds of cellulose is measured to be 79% (sample a),  
250 80% (sample b), 77% (sample c) and 73% (sample d), respectively, using Segal's empirical  
251 method. The results indicate that the mechanical treatment caused little damage to the crystalline  
252 character of the cellulose during melt compounding. In addition, a new weak peak at  $2\theta=18.8^\circ$   
253 ascribing to the 130 plane of residual PP is observed in the spectrum of sample c.<sup>38</sup> This result  
254 further confirmed the strong interfacial interactions between the modified PP and TBCF.

255 The thermal properties of cellulose fibers is important to their applications in polymer  
256 composites, wherein the processing temperature for thermoplastic polymers is usually above 200  
257 °C.<sup>39</sup> The melt compounded composites were etched by the Soxhlet extraction method using  
258 toluene as solvent for 5 days to remove the PP matrix. The TG and DTG curves of TBCF (a),  
259 TBCF extracted from neat PP/TBCF composites (b), TBCF extracted from modified PP/TBCF  
260 composites (c), BCF extracted from modified PP/BCF composites (d) and neat PP (e) are shown  
261 in Fig. 7. As can be seen, the onset decomposition temperature of five samples is 287.4, 284.7,

262 284.9, 265.4 and 407.3 °C, respectively. The result indicates that the bamboo fiber used in this  
263 study has excellent thermal stability and its structure was not destroyed by the mechanical  
264 shearing during melt compounding, implying that the cellulose derived from this quickly grown  
265 plants is a promising inexpensive reinforcement for polymer composites. In comparison with  
266 sample b and d, the thermal degradation peak of residual PP at 400-480 °C can be clearly observed  
267 in the DTG curve of sample c, which is consistent with the thermal degradation temperature of  
268 neat PP (sample e). The amount of modified PP which has strong interactions with TBCF can be  
269 calculated from the TGA results. Cellulose was almost completely decomposed below 400 °C as  
270 shown in the TGA curves (sample a). Therefore, the approximately 5 wt% weight loss above 400  
271 °C of the modified PP/TBCF composites (sample c) is attributed to the strongly combined PP onto  
272 TBCF after melt compounding, suggesting an enhanced interfacial adhesion between TBCF and  
273 modified PP matrix.

274 In order to intuitively explain the aforementioned results, the SEM images of neat BCF, BCF  
275 extracted from modified PP/BCF composites and TBCF extracted from modified PP/TBCF  
276 composites are shown in Fig. 8. It is observed that the morphology of BCF extracted from  
277 modified PP/BCF composites is very similar to that of neat BCF (as shown in Fig. 8a). There is no  
278 residual PP on the surface of BCF which indicated the weak interfacial adhesion. However, Fig. 8c  
279 shows that a number of residual PP is adhered firmly on the surface of TBCF extracted from  
280 modified PP/TBCF composites, attributing to the strong interfacial interaction between modified  
281 PP and TBCF.

### 282 **3.4 Mechanical properties of PP/cellulose composites**

283 Typically, the enhanced interfacial interaction has a positive impact on the mechanical

284 properties of PP/cellulose composites.<sup>40</sup> Since tensile strength is more dependent upon the  
285 polymer/cellulose interfacial interaction than tensile modulus,<sup>41</sup> the effect of mechanochemical  
286 modification and TEMPO-mediated oxidation on the tensile strength of PP/cellulose composites  
287 was shown in Fig. 9 and discussed in detail. The tensile strength of neat PP/TBCF composites  
288 dropped sharply with the increase of fiber loading due to the weak interfacial interaction between  
289 fiber and matrix.<sup>42, 43</sup> In contrast, the tensile strength of modified PP/BCF composites improved  
290 obviously with the same fiber content. When the fiber content was increased, BCF was directly  
291 contact with one another and aggregated in the polymer matrix becoming fracture origins during  
292 mechanical testing. Islam et al.<sup>44</sup> reported that the tensile strength of the composites prepared from  
293 chemically treated coir decreased beyond 10 wt% fiber content. However, in our work, the tensile  
294 strength of modified PP/TBCF composites increased greatly and this effect is more evident at  
295 higher fiber content. The tensile strength of neat PP/TBCF and modified PP/BCF composites with  
296 50 wt% cellulose is 21.8 and 30.1 MPa, while that of the modified PP/TBCF composite with 50  
297 wt% cellulose is significantly increased to 46.3 MPa. The remarkable increase of tensile strength  
298 can be ascribed to the synergistic effect of the combination of mechanochemical modification of  
299 PP and TEMPO-mediated oxidation of cellulose. The MA moieties effectively bonded with the  
300 reactive hydroxyl groups on the cellulose surface, ensuing more efficient load transfer, thereby  
301 prevented crack growth and enhanced the mechanical properties.<sup>45</sup>

302

#### 303 **4. Conclusion**

304 In this study, we demonstrated that the combination of the mechanochemical modification  
305 and TEMPO-mediated oxidation can be used as an effective approach to establish strong

306 interfacial interaction between cellulose and PP matrix. The released reactive hydroxyl groups on  
307 the fiber surface generated by TEMPO-mediated oxidation processing effectively bonded with  
308 MAH-modified PP and thus created a strong interfacial adhesion. FTIR, XRD and TGA analysis  
309 indicated that approximately 5 wt% modified PP was tightly attached to TBCF and could not be  
310 removed even after 120 h of Soxhlet extraction by dimethylbenzene. The present investigation  
311 showed the feasibility of producing high performance cellulose fiber-reinforced polymer  
312 composites with remarkably improved mechanical properties, which can have potential  
313 applications in the near future.

314

### 315 **Acknowledgments**

316 The authors would like to thank the National Science Foundation of China (51473100 and  
317 51203105) for financial support.

318

### 319 **References**

- 320 1 P. R. Charani, M. Dehghani-Firouzabadi, E. Afra, A. Blademo, A. Naderi and T. Lindström,  
321 *Cellulose*, 2013, **20**, 2559-2567.
- 322 2 J. Li, X. Wei, Q. Wang, J. Chen, G. Chang, L. Kong, J. Su and Y. Liu, *Carbohydr. Polym.*, 2012,  
323 **90**, 1609-1613.
- 324 3 U. Ratanakamnuan, D. Atong and D. Aht-Ong, *Carbohydr. Polym.*, 2012, **87**, 84-94.
- 325 4 I. F. Pinheiro, A. R. Morales and L. H. Mei, *Cellulose*, 2014, **21**, 4381-4391.
- 326 5 X. Xiao, S. Lu, B. Qi, C. Zeng, Z. Yuan and J. Yu, *RSC Adv.*, 2014, **4**, 14928-14935.
- 327 6 M. Zhou, J. Yan, Y. Li, C. Geng, C. He, K. Wang and Q. Fu, *RSC Adv.*, 2013, **3**, 26418-26426.

- 328 7 S. Y. Lee, S. J. Chun, G. H. Doh, I. A. Kang, S. Lee and K. H. Paik, *J. Compos. Mater.*, 2009, **43**,  
329 1639-1657.
- 330 8 S. Virtanen, J. Vartianen, H. Setälä, T. Tammelin, S. Vuoti, *RSC Adv.*, 2014, **4**, 11343-11350.
- 331 9 M. M. Ibrahim, W. K. El-Zawawy and M. A. Nassar, *Carbohydr. Polym.*, 2010, **79**, 694-699.
- 332 10 W. Qiu, F. Zhang, T. Endo and T. Hirotsu, *Polym. compos.*, 2005, **26**, 448-453.
- 333 11 D. R. Mulinari, H. J. C. Voorwald, M. O. H Cioffi, M. L. C. da Silva, T. G. da Cruz and C.  
334 Saron, *Compos. Sci. Technol.*, 2009, **69**, 214-219.
- 335 12 S. L. Fávaro, M. S. Lopes, A. G. Vieira de Carvalho Neto, R. Rogério de Santana and E.  
336 Radovanovic, *Compos. Part A-Appl. S.*, 2010, **41**, 154-160.
- 337 13 S. Iwamoto, S. Yamamoto, S. H. Lee and T. Endo, *Compos. Part A-Appl. S.*, 2014, **59**, 26-29.
- 338 14 D. Tian, X. Zhang, C. Lu, G. Yuan, W. Zhang and Z. Zhou, *Cellulose*, 2014, **21**, 473-484.
- 339 15 X. Zhang, Z. Lu, D. Tian, H. Li and C. Lu, *J. Appl. Polym. Sci.*, 2013, **127**, 4006-4014.
- 340 16 Z. Zhou, X. Zhang, D. Tian, R. Xiong and C. Lu, *Mater. Res. Innov.*, 2013, **17**, 84-91.
- 341 17 A. K. Bledzki, A. A. Mamun, M. Lucka-Gabor and V. S. Gutowski, *Express. Polym. Lett.*, 2008,  
342 **2**, 413-422.
- 343 18 X. Zhang, C. Lu and M. Liang, *J. Appl. Polym. Sci.*, 2007, **103**, 4087-4094.
- 344 19 X. Zhang, C. Chen and C. Li, *Prog. Rubber. Plast. Re.*, 2012, **28**, 81-93.
- 345 20 T. Saito and A. Isogai, *Biomacromolecules*, 2004, **5**, 1983-1989.
- 346 21 C. Li, Y. Zhang and Y. Zhang, *Polym. Test.*, 2003, **22**, 191-195.
- 347 22 L. G. J. M. A. Segal, J. J. Creely, A. E. Martin and C. M. Conrad, *Text. Res. J.*, 1959, **29**,  
348 786-794.
- 349 23 X. He, X. Zhang, W. Zhang, D. Tian and C. Lu, *J. Viny. Addit. Technol.*, 2014, **20**, 177-184.

- 350 24 M. A. Chen, H. Z. Li, X. H. Zhang, *Int. J. Adhes.*, 2007, **27**, 175-187.
- 351 25 X. Zhang, C. Lu and M. Liang, *J. Polym. Res.*, 2009, **16**, 411-419.
- 352 26 X. Zhang, C. Lu, Q. Zheng and M. Liang, *Polym. Adv. Technol.*, 2011, **22**, 2104-2109.
- 353 27 T. Saito, M. Hirota, N. Tamura, S. Kimura, H. Fukuzumi, L. Heux and A. Isogai,  
354 *Biomacromolecules*, 2009, **10**, 1992-1996.
- 355 28 A. Isogai, T. Saito and H. Fukuzumi, *Nanoscale*, 2011, **3**, 71-85.
- 356 29 T. Saito, S. Kimura, Y. Nishiyama and A. Isogai, *Biomacromolecules*, 2007, **8**, 2485-2491.
- 357 30 W. Chen, K. Abe, K. Uetani, H. Yu, Y. Liu and H. Yano, *Cellulose*, 2014, **21**, 1517-1528.
- 358 31 N. M. L. Hansen, T. O. J. Blomfeldt, M. S. Hedenqvist and D. V. Plackett, *Cellulose*, 2012, **19**,  
359 2015-2031.
- 360 32 M. O. Adebajo and R. L. Frost, *Spectrochim. Acta. A.*, 2004, **60**, 2315-2321.
- 361 33 H. Xia, Q. Wang, K. Li and G. Hu, *J. Appl. Polym. Sci.*, 2004, **93**, 378-386.
- 362 34 H. S. Yang, H. J. Kim, H. J. Park, B. J. Lee and T. S. Hwang, *Compos. Struct.*, 2007, **77**, 45-55.
- 363 35 L. M. Matuana, J. J. Balatinecz, R. N. S. Sodhi and C. B. Park, *Wood Sci. Technol.*, 2001, **35**,  
364 191-201.
- 365 36 M. Kazayawoko, J. J. Balatinecz and R. T. Woodhams, *J. Appl. Polym. Sci.*, 1997, **66**,  
366 1163-1173.
- 367 37 S. Alila, I. Besbes, M. R. Vilar, P. Mutjé and S. Boufi, *Ind. Crop. Prod.*, 2013, **41**, 250-259.
- 368 38 M. R. Meng and Q. Dou, *Mater. Sci. Eng. A-Struct.*, 2008, **492**, 177-184.
- 369 39 J. Wang, Q. Cheng, L. Lin and L. Jiang, *ACS Nano*, 2014, **8**, 2739-2745.
- 370 40 N. Lin, S. Wei, T. Xia, F. Hu, J. Huang and A. Dufresne, *RSC Adv.*, 2014, **4**, 49098-49107.
- 371 41 L. Zhong, S. Fu, X. Zhou and H. Zhan, *Compos. Part A-Appl. S.*, 2011, **42**, 244-252.

- 372 42 M. M. Haque, M. Hasan, M. S. Islam, M. E. Ali, *Bioresource Technol.*, 2009, **100**, 4903-4906.
- 373 43 X. Colom, F. Carrasco, P. Pages, J. Canavate, *Compos. Sci. Technol.*, 2003, **63**, 161-169.
- 374 45 M. N. Islam, M. R. Rahman, M. M. Haque, M. M. Huque, *Composites Part A-Appl. S.*, 2010,
- 375 **41**, 192-198.
- 376 45 K. B. Adhikary, S. Pang and M. P. Staiger, *Compos. Part B-Eng.*, 2008, **39**, 807-815.
- 377
- 378
- 379
- 380
- 381
- 382
- 383
- 384
- 385
- 386
- 387
- 388
- 389
- 390
- 391
- 392
- 393

394 **Figure captions**

395 **Fig. 1** Schematic illustration for the preparation of modified PP/TBCF composite through dual modification.

396 **Fig. 2** Optical micrographs of modified PP powder (a), TBCF (b) and SEM images of neat PP/TBCF composite (c),  
397 modified PP/BCF composite (d) and modified PP/TBCF composite (e) with 30 wt% cellulose.

398 **Fig. 3** XPS wide-scan and C 1s spectra of neat PP and modified PP.

399 **Fig. 4** Dynamic water contact angles of neat PP and modified PP.

400 **Fig. 5** FTIR spectra of TBCF (a), cellulose extracted from neat PP/TBCF composites (b) and modified PP/TBCF  
401 composites (c).

402 **Fig. 6** XRD patterns of TBCF (a), TBCF extracted from neat PP/TBCF composites (b), TBCF extracted from  
403 modified PP/TBCF composites (c) and BCF extracted from modified PP/BCF composites (d).

404 **Fig. 7** TG and DTG curves of TBCF (a), TBCF extracted from neat PP/TBCF composites (b), TBCF extracted  
405 from modified PP/TBCF composites (c), BCF extracted from modified PP/BCF composites (d) and neat PP (e).

406 **Fig. 8** The SEM images of neat BCF (a), BCF extracted from modified PP/BCF composites (b) and TBCF  
407 extracted from modified PP/TBCF composites (c).

408 **Fig. 9** Tensile strength of neat PP/TBCF, modified PP/TBCF and modified PP/BCF composites.

409

410

411

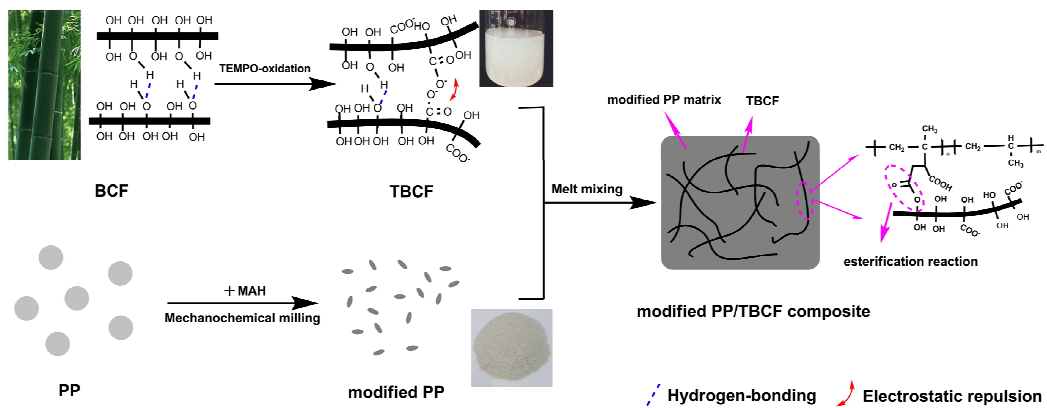
412

413

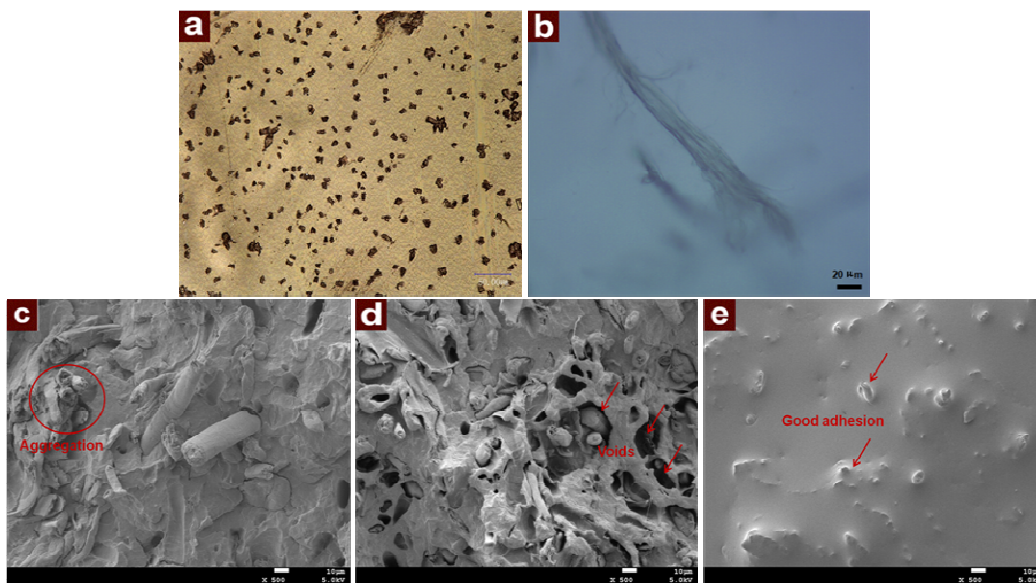
414

415

416 **Fig. 1** Schematic illustration for the preparation of modified PP/TBCF composite through dual modification.



434 **Fig. 2** Optical micrographs of modified PP powder (a), TBCF (b) and SEM images of neat PP/TBCF composite (c),  
435 modified PP/BCF composite (d) and modified PP/TBCF composite (e) with 30 wt% cellulose.



436

437

438

439

440

441

442

443

444

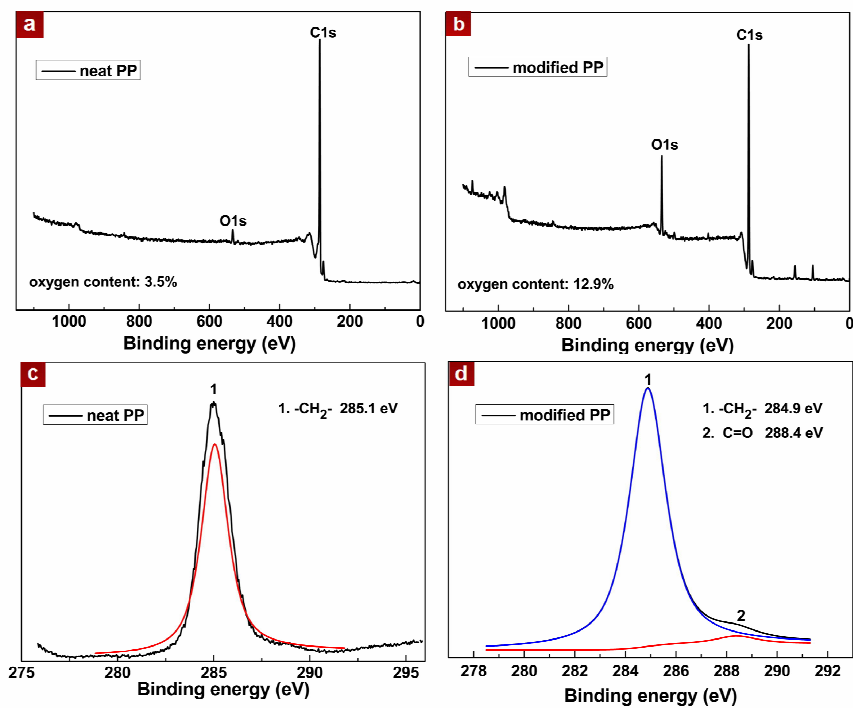
445

446

447

448

449

450 **Fig. 3** XPS wide-scan and C 1s spectra of neat PP and modified PP.

451

452

453

454

455

456

457

458

459

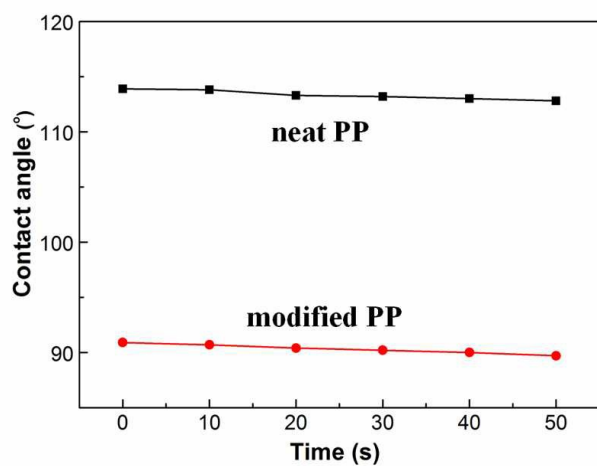
460

461

462

463

464 **Fig. 4** Dynamic water contact angles of neat PP and modified PP.



465

466

467

468

469

470

471

472

473

474

475

476

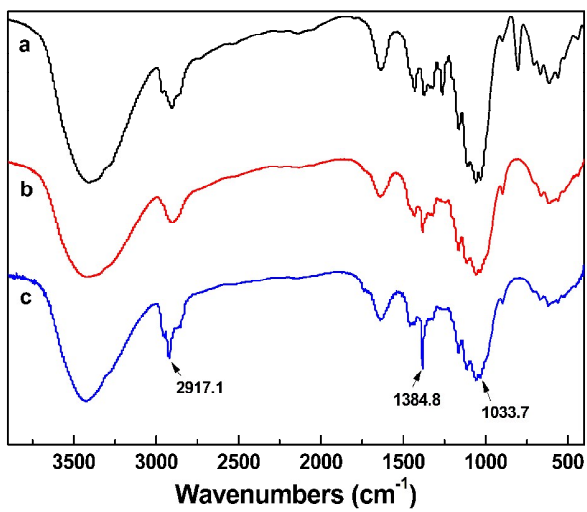
477

478

479

480

481 **Fig. 5** FTIR spectra of TBCF (a), cellulose extracted from neat PP/TBCF composites (b) and modified PP/TBCF  
482 composites (c).



483

484

485

486

487

488

489

490

491

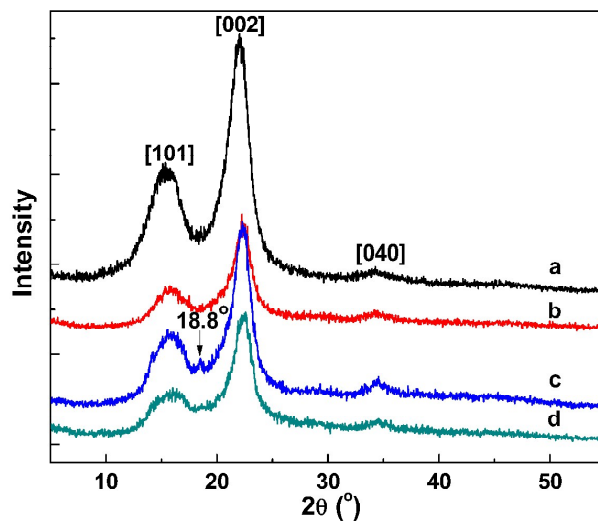
492

493

494

495

496 **Fig. 6** XRD patterns of TBCF (a), TBCF extracted from neat PP/TBCF composites (b), TBCF extracted from  
497 modified PP/TBCF composites (c) and BCF extracted from modified PP/BCF composites (d).



498

499

500

501

502

503

504

505

506

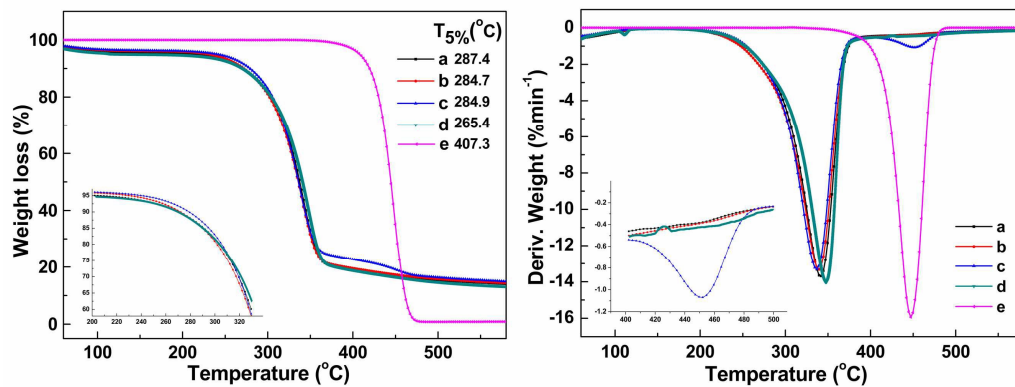
507

508

509

510

511 **Fig. 7** TG and DTG curves of TBCF (a), TBCF extracted from neat PP/TBCF composites (b), TBCF extracted  
512 from modified PP/TBCF composites (c), BCF extracted from modified PP/BCF composites (d) and neat PP (e).



513

514

515

516

517

518

519

520

521

522

523

524

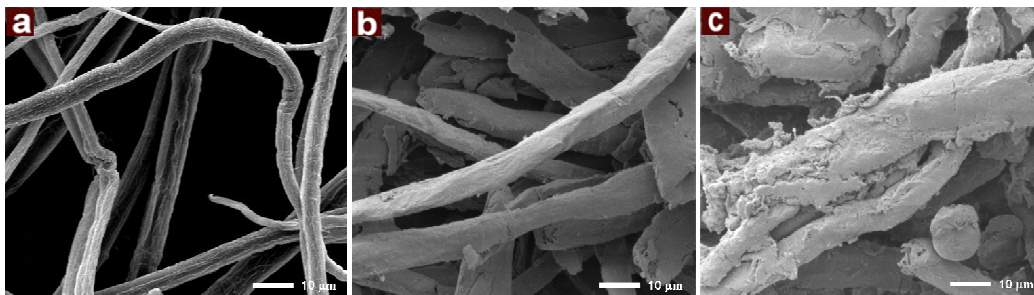
525

526

527

528

529 **Fig. 8** The SEM images of neat BCF (a), BCF extracted from modified PP/BCF composites (b) and TBCF  
530 extracted from modified PP/TBCF composites (c).



531

532

533

534

535

536

537

538

539

540

541

542

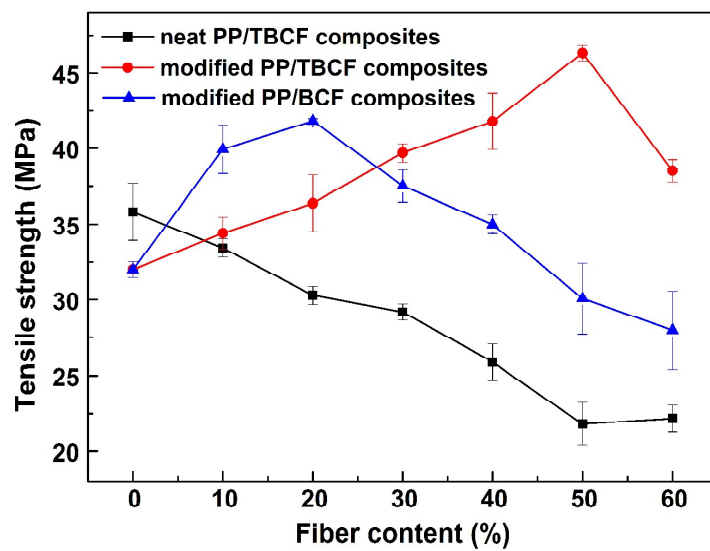
543

544

545

546

547

548 **Fig. 9** Tensile strength of neat PP/TBCF, modified PP/TBCF and modified PP/BCF composites.

549

550

551

552